How to cite: *Angew. Chem. Int. Ed.* **2020**, *59*, 16114–16121
International Edition: doi.org/10.1002/anie.202005269
German Edition: doi.org/10.1002/ange.202005269

Intersystem Crossing

Elucidation of the Intersystem Crossing Mechanism in a Helical BODIPY for Low-Dose Photodynamic Therapy

Zhijia Wang[+], Ling Huang[+], Yuxin Yan[+], Ahmed M. El-Zohry, Antonio Toffoletti, Jianzhang Zhao, Antonio Barbon,* Bernhard Dick,* Omar F. Mohammed,* and Gang Han**

Abstract: *Intersystem crossing (ISC) of triplet photosensitizers is a vital process for fundamental photochemistry and photodynamic therapy (PDT). Herein, we report the co-existence of efficient ISC and long triplet excited lifetime in a heavy atom-free bodipy helicene molecule. Via theoretical computation and time-resolved EPR spectroscopy, we confirmed that the ISC of the bodipy results from its twisted molecular structure and reduced symmetry. The twisted bodipy shows intense long wavelength absorption ($\varepsilon = 1.76 \times 10^5\ M^{-1}\ cm^{-1}$ at 630 nm), satisfactory triplet quantum yield ($\Phi_T = 52\ \%$), and long-lived triplet state ($\tau_T = 492\ \mu s$), leading to unprecedented performance as a triplet photosensitizer for PDT. Moreover, nanoparticles constructed with such helical bodipy show efficient PDT-mediated antitumor immunity amplification with an ultra-low dose ($0.25\ \mu g\ kg^{-1}$), which is several hundred times lower than that of the existing PDT reagents.*

[*] Dr. Z. Wang,[+] Y. Yan,[+] Prof. J. Zhao
State Key Laboratory of Fine Chemicals, School of Chemical Engineering, Dalian University of Technology
2 Ling Gong Road, Dalian 116024 (China)
E-mail: zhaojzh@dlut.edu.cn

Dr. L. Huang,[+] Prof. G. Han
Department of Biochemistry and Molecular Pharmacology
University of Massachusetts Medical School
Worcester, Massachusetts 01605 (USA)
E-mail: Gang.Han@umassmed.edu

Dr. A. M. El-Zohry, Prof. O. F. Mohammed
Division of Physical Sciences and Engineering, King Abdullah University of Science and Technology (KAUST)
Thuwal 23955-6900 (Kingdom of Saudi Arabia)
E-mail: omar.abdelsaboor@kaust.edu.sa

Dr. A. Toffoletti, Dr. A. Barbon
Dipartimento di Scienze Chimiche, Università degli Studi di Padova
Via Marzolo 1, 35121 Padova (Italy)
E-mail: antonio.barbon@unipd.it

Prof. B. Dick
Lehrstuhl für Physikalische Chemie, Institut für Physikalische und Theoretische Chemie, Universität Regensburg
Universitätsstr. 31, 93053 Regensburg (Germany)
E-mail: Bernhard.Dick@chemie.uni-regensburg.de

[+] These authors contributed equally to this work.

Supporting information and the ORCID identification number(s) for the author(s) of this article can be found under: https://doi.org/10.1002/anie.202005269.

Introduction

PDT holds great promise and has attracted considerable interest as a less invasive tumor treatment option.[1–5] When photosensitizers are photoexcited, they react with oxygen molecules in the microenvironment to produce singlet oxygen ($^1O_2$), thereby eliciting nearby tumor cell death. In this treatment, photosensitizing molecules that exhibit intense absorption of long-wavelength light, long-lived triplet states, and high singlet oxygen sensitization ability are essential for the potency of the therapy.

To date, only two porphyrin-based PDT reagents have been approved by FDA for clinical cancer treatment.[6] However, due to their low absorption for deep-tissue-penetrable long-wavelength light and subsequent suboptimal singlet oxygen sensitization ability, high doses of these PDT reagents are required for operation. For example, PpIX has a low molar absorption efficiency ($\varepsilon < 5000\ M^{-1}\ cm^{-1}$) at 635 nm. Hence, high concentrations (40 mg kg^{-1}–200 mg kg^{-1}) of 5-aminolevulinic acid (ALA, the precursor of PpIX) are required for PDT treatment.[7] Moreover, due to the low molar absorption coefficient ($\varepsilon \approx 1170\ M^{-1}\ cm^{-1}$) at 630 nm, Photofrin, the other FDA approved PDT reagent in clinical practice, also suffers from the same problem of requiring high doses for PDT treatment.[1,7] There are great concerns that the use of such high doses of photosensitizers can lead to prolonged undesired patient photosensitivity and certain side effects such as acid reflux, nausea, and flushing sensation.[6,8]

In order to reduce the required drug dose, significant efforts have been made to develop non-porphyrin PDT reagents that have strong absorption of long-wavelength light and high singlet oxygen quantum yield. Yet, to date, the effective long-wavelength-light-absorbing photosensitizers have to rely on heavy atoms to improve their ISC (the transition from the singlet to triplet state) and consequent singlet oxygen generation.[9,10] For instance, metal complexes (Pt, Ru, Ir)[11–15] and brominated/iodinated chromophores[16] are reported. Unfortunately, besides the potential toxicity of these heavy atoms, the dilemma here is that the improvement of the $S_1 \rightarrow T_n$ ISC is often at the cost of reducing the triplet state lifetime, as the undesired $T_1 \rightarrow S_0$ ISC (decay of the triplet excited state) can be enhanced by the heavy atom effect as well,[9] which is especially significant for those long-wavelength-absorbing photosensitizers (Supporting Information, Table S2). Such a shortened triplet lifetime curtailed the reaction duration of oxygen and PDT reagents, thus being detrimental for singlet oxygen generation and concomitant

PDT, especially for hypoxic environments such as those in tumors (Figure S9).[4]

To overcome this challenge, in this work, we sought to explore the possibility to develop metal/heavy atom-free long-wavelength-absorbing triplet photosensitizers that have both satisfactory triplet state quantum yield and uncompromised long triplet excited state lifetime. Currently, heavy atom-free photosensitizers are known to have much longer triplet lifetime[17] but usually poor ISC.[5] Efficient long-wavelength heavy atom-free triplet photosensitizers are rare (Table S3). In this study, we got inspiration from distorted conjugated systems, which display elevated ISC efficiency.[18–26] In particular, the removal of the mirror-plane symmetry of a planar π-system is considered to allow for a stronger spin orbit coupling (SOC) between π–π* states with different spin manifolds (the singlet state and triplet state), hence facilitating ISC.[27] The most notable exemplar molecule is the buckminsterfullerene (C_{60}), which has a heavily curved π-conjugation skeleton. This molecule was reported to show unity ISC efficiency but has only an extremely low molar extinction coefficient in the visible spectral range.[21] Another exemplar are helicenes. Helicenes are helical compounds made of twisted *ortho*-fused aromatic rings, which have been known to have an excellent ISC effect.[27] Yet, most existing helicenes only absorb ultraviolet light, and it has been quite challenging to shift absorption towards the visible/near-infrared region.[28–31]

Herein, we report on the discovery of the co-existence of satisfactory triplet state quantum yield and long triplet lifetime in a heavy atom-free helicene molecule, based on a strong and robust visible-light-harvesting bodipy chromophore (**helical-BDP**, Figure 1). In particular, such a heavy atom-free molecule exhibits the co-existence of satisfactory triplet quantum yield (ISC quantum yield $\Phi_T = 52\,\%$) and the long-lived triplet state (492 μs), as well as exceptionally intense absorption in the long-wavelength range (molar absorption coefficient $\varepsilon = 1.76 \times 10^5\,M^{-1}\,cm^{-1}$ at 630 nm). The ISC mechanism of this heavy atom-free molecule was elucidated by investigating the selective population of triplet excited state sublevels during ISC by time-resolved electron paramagnetic resonance (TR-EPR) spectroscopy and advanced theoretical computations. Moreover, by encapsulating such a triplet photosensitizer in a nanoparticle, the helical bodipy nanoparticles showed surprisingly highly efficient PDT-augmented anti-PD-L1 antitumor immunity, with a record low dose (0.25 $\mu g\,kg^{-1}$). This dose is hundred times lower than that of the PDT reagents used in the clinic and reported in the literature (at least 0.1 $mg\,kg^{-1}$, Tables S1 and S4).

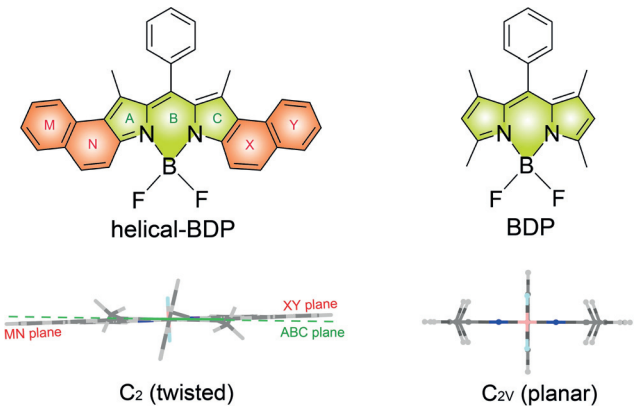

Figure 1. Molecular structures of **helical-BDP** and **BDP** (top) and the side view of the RHF optimized ground structures (bottom).

Results and Discussion

Molecular Structures

Inspired by the ISC ability of helicene and the lack of long-wavelength-absorbing helicenes,[31,32] we were prompted to seek new helicene structures that are based on long-wavelength-light-harvesting chromophores and explore their ISC properties. Bodipy is a popular fluorophore for its large molar absorption coefficient, bright fluorescence, and excellent stability. In this regard, we scrutinized few reported bodipy derivatives with twisted π-conjugation planes (previously synthesized only as fluorophore candidates and the ISC properties were not studied).[32–35] Among these, through theoretical computations, we identified that a π-conjugation framework of the naphthalene-fused bodipy derivative (**helical-BDP**, Figure 1), previously reported by Shen et al,[35] is twisted in a way that is similar to that of helicene.[36–38] As shown in Figure 1, there is a small but notable angle between the planes shown in green and orange. This geometry is distinctly different from the unsubstituted bodipy (**BDP**, Figure 1), and those substituted bodipy derivatives that have a strictly planar extended π-conjugation framework,[39] which are known to have negligible ISC.[40]

With the intuition that this helical-twisted molecule (**helical-BDP**, Figure 1) should inherit the strong ISC ability from helicene, we explored its ISC capability, triplet lifetime, and potential for PDT. The **helical-BDP** was prepared based on reported methods.[35] We observed the outstanding ISC of this twisted molecule by both nanosecond transient absorption (ns-TA) spectroscopy and singlet oxygen photosensitizing experiments. The ISC mechanism for this twisted heavy atom-free molecule was further revealed through TR-EPR and theoretical computations. The parent bodipy (**BDP**, Figure 1) was used as a control compound throughout this study.

Photophysical Study: Absorption, Triplet Excited States, and ISC Kinetics

The absorption band of the **helical-BDP** is centered at 630 nm, with the molar absorption coefficient ($1.76 \times 10^5\,M^{-1}\,cm^{-1}$) almost twice that of **BDP** (Figure 2a). Moreover, the vibrational progression of the **helical-BDP** is more resolved than that of the **BDP**. Our results demonstrate that the twisted structure clearly altered the excited state properties of the bodipy chromophore.

The triplet excited state of the **helical-BDP** was investigated by ns-TA spectroscopy (Figure 2b). In particular, upon pulsed laser excitation at 628 nm, two negative bands

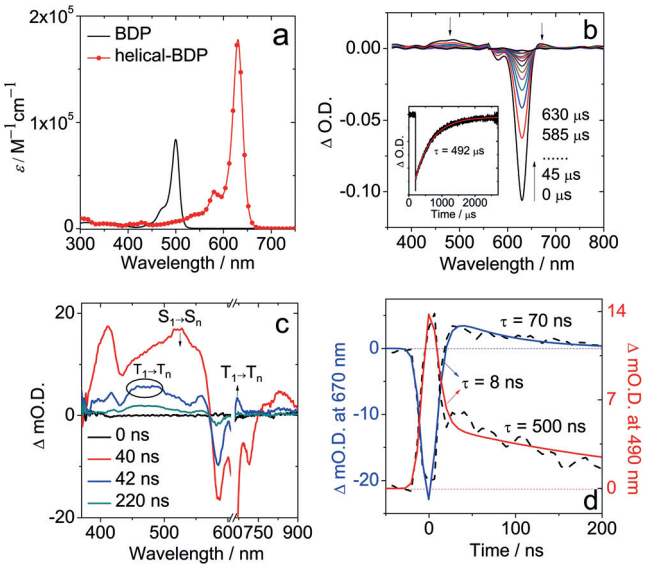

Figure 2. Steady-state and transient absorption spectroscopies. a) Molar extinction coefficient of **helical-BDP** in DCM. b) ns-TA spectra of **helical-BDP** ($\lambda_{ex}=628$ nm, $c=1.25\times10^{-6}$ M). Inset: Decay trace of **helical-BDP** at 610 nm, $c=3.1\times10^{-7}$ M. This was measured in deaerated DCM, recorded in the co-linear measurement mode of the LP980 ns-TA spectrometer, 20 °C. c) ns-TA spectra of **helical-BDP** in toluene ($\lambda_{ex}=640$ nm) at 0 ns, 40 ns, 42 ns and 220 ns. The arrows indicate the evolution of various bands. d) The kinetic trace at 670 nm and 490 nm show the time constant for triplet state formation.

centered at 625 nm and 579 nm were observed. These are the two ground state bleaching bands (GSB, see the steady state absorption of the compound, Figure 2a). In addition, a weak excited state absorption (ESA) band in the range of 400–550 nm was observed. This is attributed to the absorption of the T_1 triplet state ($T_1\rightarrow T_n$ transition). Moreover, by monitoring the decay of the GSB signal at 610 nm, the triplet excited state was found to be long-lived (hundreds of microseconds) in deaerated solution (inset of Figure 2b). In contrast, in an aerated solution, the lifetime was greatly reduced to 224 ns (Figure S2). Such a significant reduction in its lifetime clearly confirmed the triplet state feature of the transient species.

Notably, the intrinsic triplet state lifetime ($\tau=492$ μs, for details, see Supporting Information) is much longer than that of typical heavy atom-containing triplet photosensitizers showing long-wavelength absorption (Table S2, for instance, $\tau_T=1.7$ μs for the 2,6-diiodo-bisstyrylbodipy). It should be noted that heavy-atom photosensitizers tend to have a significantly reduced triplet state lifetime (heavy-atom effect), which is especially severe for chromophores that have long-wavelength absorption with low triplet energy. For instance, with iodination, the triplet lifetime of 3,5-distyrylbodipy was significantly reduced from 72 μs to 1.7 μs (Table S2). Such a shortened triplet lifetime is detrimental to applications, such as oxygen sensing,[41] photocatalysis[42] and PDT,[4] as these applications are all based on intermolecular diffusion-controlled triplet energy transfer or electron transfer, for which the efficiency is dependent on the triplet state lifetimes of the photosensitizer. Our study shows that the $^1O_2$ sensitization ability (a basic process in PDT) of a triplet photosensitizer showing a short-lived triplet state almost vanishes in hypoxic conditions; the singlet oxygen quantum yield drops from 45% under normal conditions to 2% under a hypoxic atmosphere. However, this did not occur for the long-lived **helical-BDP** ($\Phi_\Delta\approx36\%$ in both normal atmosphere and hypoxic atmosphere, Figure S9). Hence, the long triplet state lifetime of the helical bodipy shows its unique advantage over the conventional method of using the heavy-atom effect. Inspired by the excellent photophysical properties of **helical-BDP**, we explored the feasibility of TTA upconversion by using this special heavy atom-free photosensitizer. Outstanding overall red-to-yellow TTA upconversion brightness was obtained ($\eta=\varepsilon\Phi_{UC}=1296\,M^{-1}cm^{-1}$ at 250 mW cm^{-2} of 635 nm excitation) with **helical-BDP** as an intense red-light-absorbing photosensitizer in conjunction with perylenebisimide (PBI) as the yellow emitter (Figures S5 and S6).

In order to study the kinetics of ISC, ns-TA spectroscopy with higher time resolution was performed. As shown in Figure 2c, the ESA at 525 nm is attributed to the $S_1\rightarrow S_n$ absorption band. At a longer delay time (42 ns in Figure 2c), the shape of the spectrum resembles that of Figure 2b, clearly showing that the ISC process takes place. Hence, the ESA bands centered at 490 nm and 670 nm can be attributed to the $T_1\rightarrow T_n$ absorption. The ISC time constant for **helical-BDP** was determined to be $1/k_{ISC}=8$ ns (Figure 2d). According to the population ratio of the sublevels of the triplet state measured by TR-EPR spectra ($P_x/P_y/P_z=1:0:0.2$, see later section, Figure 4c), the electron spin-selective ISC rate constants (k_{ISC}) to the triplet sublevels (T_x, T_y, T_z) of the T_1 state are 0.10 ns^{-1}, 0 ns^{-1}, and 0.02 ns^{-1}, respectively. The photophysical parameters of the compounds are listed in Table 1.

Table 1: Photophysical parameters of the compounds.[a]

Compounds	λ_{abs}[b]	ε[c]	λ_{em}[d]	τ_F[e]	Φ_F[f]	τ_T[g]	Φ_Δ[h]	Φ_T[i]
helical-BDP	630	17.6	649	3.3	21%	492	36%	52%
BDP	500	8.4	512	4.1	52%	–[j]	–[j]	–[j]

[a] In dichloromethane (DCM), 25 °C. [b] Maximum absorption wavelength, in nm. [c] Molar absorption coefficient, $10^4\,M^{-1}cm^{-1}$. [d] Maximum fluorescence emission wavelength, in nm. [e] Luminescence lifetimes, in nanoseconds (ns). [f] Fluorescence quantum yield with methyl blue as standard ($\Phi_F=3\%$ in MeOH). [g] Intrinsic triplet excited state lifetime, in microseconds (μs), $c=3.1\times10^{-7}$ M, low concentration was used to reduce the self-quenching effect. [h] Singlet oxygen quantum yield with methyl blue as standard ($\Phi_\Delta=57\%$ in DCM). [i] Triplet quantum yield determined by ns-TA spectroscopy, by triplet-triplet energy transfer method, with Methyl Blue as standard ($\Phi_T=50\%$ in MeOH). [j] Not observed.

ISC Mechanism: Theoretical Computation and TR-EPR Spectroscopy

The geometries of the compounds were examined with the intuition that they are pivotal to the ISC. Theoretical computations[43,44] show that the optimized ground-state geometry of **BDP** has C_{2v} geometry (the π-conjugation of the Bodipy chromophore is planar); while for the **helical-BDP**, the C_2 geometry is most stable, followed closely by the

C_S geometry (both are non-planar geometries, Table S7), whereas the C_{2v} geometry is a transition state.

In order to find out the relationship between the twisted structure and the enhanced ISC, the spin-orbit coupling (SOC) matrix elements between S_1 state and the sublevels (T_x, T_y, and T_z) of each triplet excited state were further determined by quantum chemical calculations (listed in Table 2). As the SOC in organic systems is considered to be

Table 2: Matrix elements (in units of cm^{-1}) of the one-electron Breit–Pauli Operator of the SOC between S_1 and the lowest two triplet states.[a]

		helical-BDP		BDP
SOC states	C_{2V}	C_2	C_S	C_{2V}
S_1/T_1	0	0.0977 *x*	0.0024 *z*	0
S_1/T_2	0	0.1689 *x*	0.0781 *z*	0

[a] Each value is labeled with the index (*x*, *y*, *z*) of the triplet sublevel. In both **helical-BDP** and **BDP**, SOC is forbidden by symmetry in the structures with C_{2v} point group (see Supporting Information for details).

a small correction to purely nonrelativistic electronic states,[27] the magnitude of the calculated SOC values (between the singlet and triplet states) reflect the possibility of ISC in a certain degree. Since T_1 is below the S_1 state, and T_2 is slightly above S_1 by approximately 0.1 eV in both the **helical-BDP** and **BDP**, both $S_1 \rightarrow T_1$ and $S_1 \rightarrow T_2$ are considered to be possible pathways of ISC (Table S7). Note that according to the CAS-Cl calculations the states S_1, T_1 and T_2 share the same symmetry.

The selection rules for SOC between a singlet state S and a triplet state T require that the product of the irreducible representation of the spatial symmetries of these two states transform like one of the three rotations [see Supporting Information for details; Equation (1)]:

$$\Gamma(\mathrm{S}) \times \Gamma(\mathrm{T}) = \Gamma(\mathrm{R}_x, \mathrm{R}_y, \mathrm{R}_z) \quad (1)$$

As a consequence, in molecules with C_{2v} geometry, SOC is forbidden between singlet and triplet states with the same spatial symmetry. Hence, SOC between S_1/T_1 or S_1/T_2 is forbidden in C_{2v} (Table 2 and Figure 3b). This rationalizes the negligible ISC ability of the parent **BDP**.

With the molecular structure deviated from the C_{2v} geometry, these selection rules will be relaxed (Figure 3a). Clearly, the magnitude of this coupling will depend on how much the twisted structures deviate from the idealized C_{2v} geometry. For the **helical-BDP**, as the C_2-geometry has the lowest energy, selective population of the T_x state is expected (see Figure 3a and Table 2). Note that T_x, T_y, T_z are three non-degenerate sublevels of the T_1 triplet state.

The overpopulation of the T_x state was experimentally confirmed by TR-EPR (Figure 4c). The spin selectivity of the ISC reflects both in the electron spin polarization (ESP) of the three sublevels of the triplet embedded in a magnetic field and in the enhanced absorption/emission (*a*/*e*) character of the main features of the TR-EPR transitions, as detailed in the Supporting Information. The TR-EPR spectrum of the triplet state of **helical-BDP** shows an (*a*, *e*, *a*, *e*, *a*, *e*) ESP

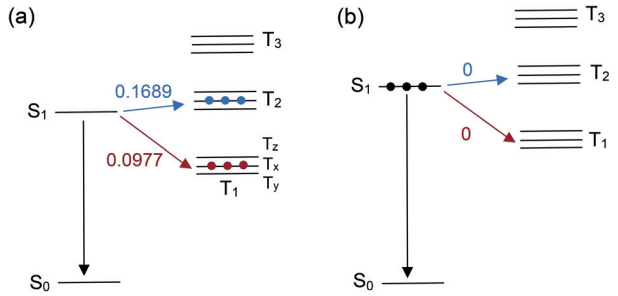

Figure 3. SOC matrix elements of the first excited singlet state with the nearest triplet states. a) SOC of **helical-BDP** in C_2 geometry and b) SOC of **BDP** in C_{2v} geometry. The labelling of the substates are indicated (note that every excited triplet state consists of three non-degenerate sublevels T_x, T_y and T_z). The larger the SOC value, the greater possibility of ISC.

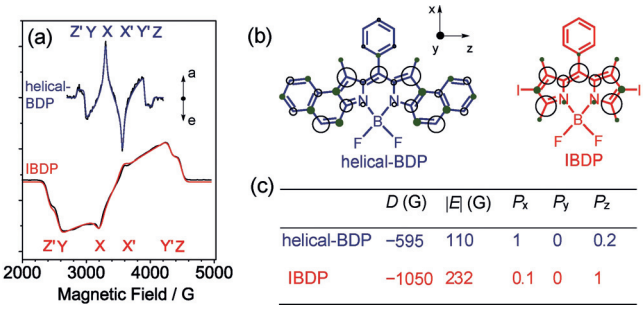

Figure 4. a) TR-EPR spectra of **helical-BDP** (λ_{ex} = 555 nm) and **IBDP** (λ_{ex} = 532 nm) in toluene/MeTHF (v/v, 3:1) frozen mixed solution, $c = 3.0 \times 10^{-5}$ M, 80 K. The canonical orientations of each transition are indicated (the prime indicates the $m_s = 0 \rightarrow m_s = +1$ transitions). b) Spin density distribution of **helical-BDP** and **IBDP**. Larger circles indicate larger (absolute) spin density value on the atom. The ZFS frame is also presented. c) Fitting parameters of the simulations in (a). P_i is the relative population of the *i*-th ZFS state, labeled as indicated in (a).

pattern (Figure 4a, blue line). A careful simulation reveals an overpopulation of the T_x state (Figure 4c). The consistency between theoretical computation and experimental TR-EPR validate that the enhanced ISC of **helical-BDP** is due to the reduced symmetry in the twisted structure. It also enables us to deduce that the **helical-BDP** possesses mainly a helical structure (C_2 geometry).

Moreover, the confinement of the triplet state wave functions of these compounds is examined, as it is crucial for rationalization of the ISC ability of the twisted structure.[27] Experimentally, the zero-field splitting (ZFS) parameter *D*-value reflects the extension of the wave functions of the two unpaired electrons of the triplet state. This value can be easily obtained from the total width of the TR-EPR spectra (see Supporting Information) of **IBDP** and **helical-BDP** (Figure 4). We clearly noticed that the width of the TR-EPR spectrum of **IBDP** is quite larger than that of the **helical-BDP** ($D = -595$ G for **helical-BDP** and $D = -1050$ G for **IBDP**, Figure 4c). We deduce that the triplet wave function of **helical-BDP** is far more delocalized than that of **IBDP**. This is supported by the calculation of the spin density distribution;

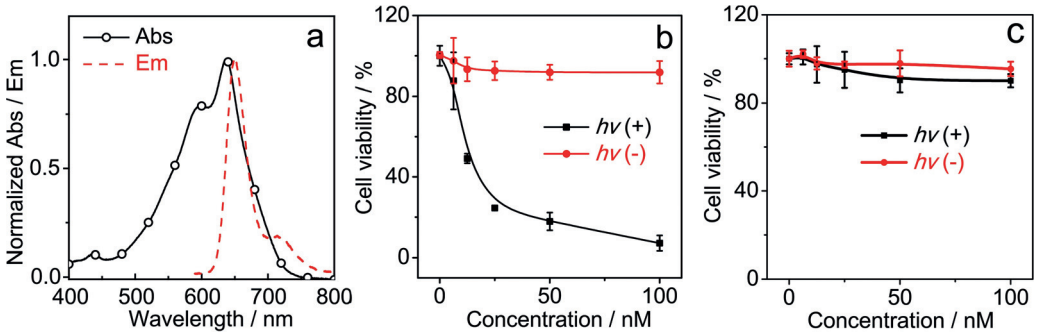

Figure 5. PDT in vitro. a) Normalized absorption and emission spectrum of **helical-BDP-NPs**. Cell viability of CT26 cells pre-treated with increasing doses of b) **helical-BDP-NPs** and c) **IRDye 700DX** with and without light irradiation. Irradiation by 656 nm LED, light dose: 6 J cm^{-2}, 20 °C.

Figure 4b shows that the wave function spreads all over the π-system of the **helical-BDP**. Hence, we have a true helical π-system. This is in agreement with the significant enhancement of ISC for the heavy atom-free **helical-BDP**; it is the delocalization of the electrons on the entire twisted molecular framework that increases the SOC for the ISC between the two π-π* states, as twisting the π-conjugation framework allows for non-vanishing one-center and two-center integrals of all atomic angular momentum operators. On the contrary, if the triplet wave function was localized on the planar π-conjugation framework as in the parent **BDP**, we would not expect any enhancement of SOC.

Record Low-Dose PDT Augmented Checkpoint Blockade Immunotherapy

Inspired by the exceptionally strong long-wavelength absorption ($\varepsilon = 1.76 \times 10^5\,M^{-1}cm^{-1}$ at 630 nm), satisfactory singlet oxygen quantum yield ($\Phi_\Delta = 36\,\%$) and the long-lived triplet state ($\tau_T = 492\,\mu s$), we explored the potential of **helical-BDP** as a long-wavelength-absorbing heavy atom-free PDT reagent to augment the checkpoint blockade immunotherapy.

Firstly, the PDT effect of **helical-BDP** on tumor cells were examined in vitro. In order to encapsulate such hydrophobic photosensitizers to be used in aqueous solution, the **helical-BDP** was wrapped in the octadecylamine substituted amphiphilic polymer (PSMA-PEG-OA) to generate such dye-loaded nanoparticles (**helical-BDP-NPs**, Figure S8). These nanoparticles showed outstanding colloidal stability (Figure S18), high dye entrapment efficiency (76 %). Their singlet oxygen quantum yields (Φ_Δ) were determined to be 21 %. The fluorescence spectrum of the **helical-BDP-NPs** is presented in Figure 5a and the fluorescence quantum yield (Φ_F) is measured to be 3.8 %. The **helical-BDP-NPs** exhibited high photocytotoxicity to the CT26 tumor cells (semi-lethal concentration $IC_{50} = 11.5$ nM) under 656 nm light irradiation, showing remarkably improved performance (Figure 5b,c) compared to the phthalocyanine photosensitizer **IRDye 700DX**, which is arguably one of the best photo-immune therapy photosensitizers.[45]

In order to study the effect of PDT mediated checkpoint blockade immunotherapy, a bilateral model of CT26 tumors on BALB/c mice was established to artificially mimic metastasis. The tumor that is treated with light illumination is considered to be the "primary tumor", and the tumor untreated at another side is considered to mimic the "metastatic tumor". As shown in Figure 6b, the mice were randomly divided into 5 groups: (1) *hv* only, (2) anti-PD-L1 only, (3) **helical-BDP-NPs** only; (4) **helical-BDP-NPs** + *hv* only, and (5) **helical-BDP-NPs** + anti-PD-L1 + *hv*. The therapeutic efficacies of different treatment groups were evaluated by measuring tumor volume.

The tumor volume growth rates of the primary tumor (treated with PDT) are presented in Figure 6e. As compared to Group 3 (only the injection of **helical-BDP-NPs**) and Group 1 (only irradiation with light, *hv*), the primary tumor in Group 4 (**helical-BDP-NPs** + *hv*) shows significant inhibition of growth, indicating that **helical-BDP-NPs** is a potent PDT reagent for primary tumors.

The tumor volume growth rates of the metastatic tumor are presented in Figure 6f. It is impressive that although the metastatic tumor was untreated with PDT, the combination of immune therapy with PDT treatment on primary tumors (Group 5 = Group 2 + Group 4) presented significant metastatic tumor suppression (Figure 6f) and obvious necrosis of metastatic tumor cells (H&E staining analysis, Figure 6d). These experimental results demonstrated that the **helical-BDP-NPs** mediated PDT can significantly augment the checkpoint blockade immunotherapy efficacy and promote abscopal effects (Figure 6a).

Specifically, anti-PD-L1 can inhibit the interaction between PD-L1 (in tumor cells) and PD-1 (in T-cells), thus rescue the T cells (Figure 6a).[46] However, this kind of checkpoint blockade immunotherapy, being only effective for tumors with the presence of T-cells, has low response rates (10–40 %).[47] On the other hand, as shown in Figure 6a, PDT can release tumor specific antigen through tumor cells apoptosis, inducing acute inflammation and increasing the infiltration of T-cells.[48–51] Hence the PDT augmented the anti-PD-L1 checkpoint blockade immunotherapy, leading to an obviously inhibition to metastatic tumor. This is verified by the analysis of the antitumor immunity. The immune cell profiling in the spleen (Figure S16) shows that the cytotoxic $CD8^+$ T cell and helper $CD4^+$ T cell levels significantly increased in the treated group (Group 5) as compared to Group 1. Moreover, in Group 5, there is a significant increase of tumor-infiltrating $CD4^+$ T-cells and $CD8^+$ T-cells in both

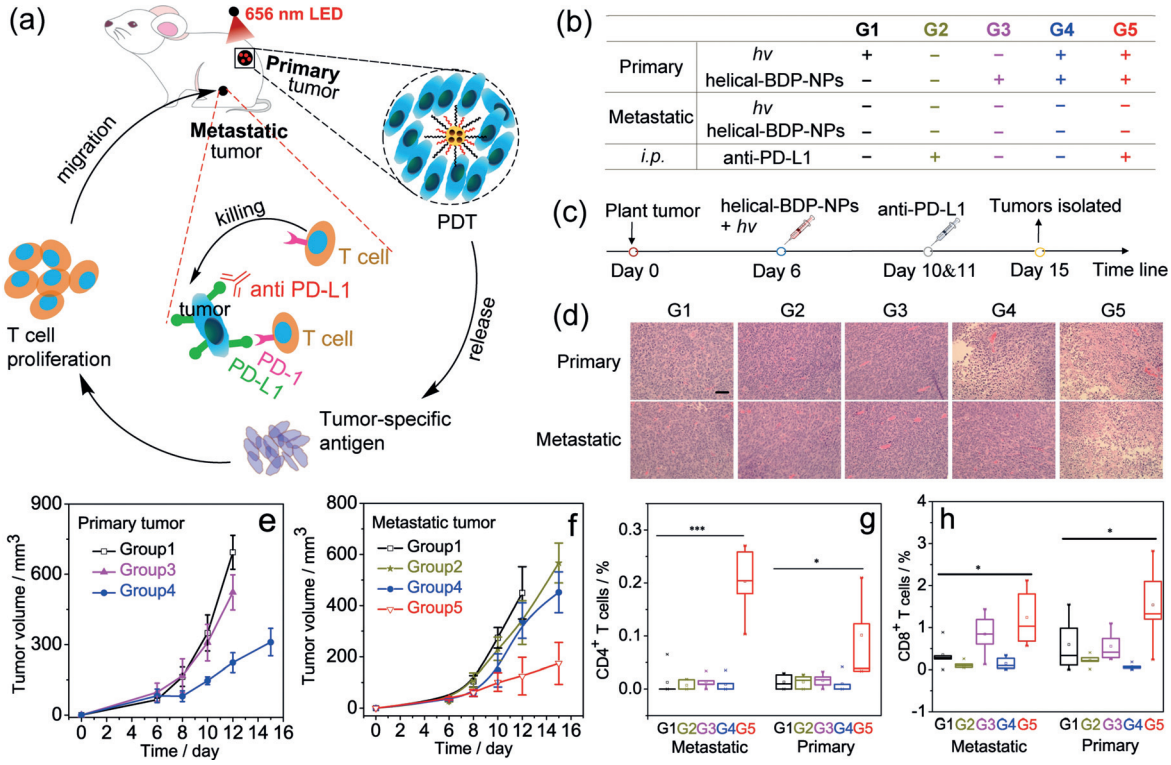

Figure 6. PDT augmented checkpoint blockade immunotherapy. a) Schematic indicating of the **helical-BDP-NPs** with anti-PD-L1 for cancer treatment. b) The experimental condition of each group (the mice were randomly divided into 5 groups). G = Group. The "+" represents the condition is satisfied and the "−" represents the condition is unsatisfied. c) Timeline of the treatment. d) Hematoxylin and eosin (H&E) staining of tumor tissue sections from different treatment groups at day 15. Scale bar = 150 μm. e) Tumor volume of primary tumor. f) Tumor volume of artificial metastatic tumor. g) Analysis the immunity $CD4^+$ T cells and h) $CD8^+$ T cells of metastatic tumor and primary tumor. Data are expressed as means ± s.d. ($n = 5$). *$P < 0.05$, **$P < 0.01$, and ***$P < 0.001$.

primary and metastatic tumors (Figure 6g,h). As a result, a significantly increased concentration of IFN-γ in Group 5 was observed (Figure S21).[52,53] These results demonstrated that the combined effect of **helical-BDP-NPs** mediated PDT and anti-PD-L1 treatment significantly increased the infiltration of effector T cells to treat the metastasis.

More importantly, to the best of our knowledge, with this novel triplet photosensitizer **helical-BDP**, PDT-mediated antitumor immunity amplification was achieved with the lowest drug dose reported to date (0.25 $\mu g\,kg^{-1}$) and an ultralow light dose (6 $J\,cm^{-2}$), being thousands of times lower than other traditional/commercial PDT reagents that have been used in the literature ($> 1.4\,mg\,kg^{-1}$, $> 18\,J\,cm^{-2}$, Table S4). The highly efficient PDT effect can be attributed to the following reasons: 1) The exceptionally high molar extinction coefficient ($\varepsilon = 1.76 \times 10^5\,M^{-1}\,cm^{-1}$ at 630 nm) enables outstanding light harvesting to occur, 2) the super-long triplet lifetime ($\tau_T = 492\,\mu s$) is critical and favorable toward achieving efficient energy transfer to produce $^1O_2$, especially in hypoxic tumors (Figure S9), and 3) the small size of the uniform spherical nanoparticles (31.5 ± 5.2 nm, Figure S10) is beneficial for their accumulation and retention in the tumor. Collectively, super-efficient PDT was achieved.

Conclusion

In summary, our results represent a new paradigm in the development of the next generation of triplet photosensitizers. For the first time, co-existence of satisfactory ISC and long triplet lifetime was revealed in a heavy atom-free bodipy helicene molecule. Advanced quantum chemical calculations and time-resolved EPR spectroscopy indicate that torsion of the plane into a helix (C_2-symmetry) enhances the ISC, yielding the population of T_x substate. Moreover, the triplet state wave function (spin-unpaired electrons) is found to be delocalized over the entire twisted π-conjugate skeleton. We showed that such a twisted bodipy helicene molecule shows exceptionally intense long-wavelength absorption ($\varepsilon = 1.76 \times 10^5\,M^{-1}\,cm^{-1}$ at 630 nm, twice that of the normal unsubstituted **BDP**), satisfactory triplet quantum yield ($\Phi_T = 52\,\%$) and a long-lived triplet state ($\tau_T = 492\,\mu s$), leading to unprecedented performance as a triplet photosensitizer. More importantly, by encapsulating such a heavy atom-free triplet photosensitizer in a nanoparticle, a record low dose of the photosensitizers (0.25 $\mu g\,kg^{-1}$) with an ultralow light dose (6 $J\,cm^{-2}$) is achieved for effective PDT immunotherapy. This dose is hundred times lower than that of the existing PDT reagents. Taken together, this heavy atom-free triplet photosensitizer shows long sought-after advantages over conventionally used triplet photosensitizers. Since ISC of organic

chromophores is fundamentally important in photochemistry as well as in many other important areas such as PDT, we believe that our study not only leads to the discovery of new heavy atom-free photosensitizer molecular structural motifs with unique triplet properties, it also opens up a wide variety of opportunities in photonic/biophotonic fields.

Acknowledgements

J.Z. thanks the NSFC (21673031, 21761142005, 21911530095 and 21421005), the State Key Laboratory of Fine Chemicals (ZYTS201901), the Fundamental Research Funds for the Central Universities (DUT19TD28), Dipartimento di Scienze Chimiche, Università degli Studi di Padova (Visiting Scientist) for support. B.D. thanks Dalian University of Technology for the Haitian Professorship support. L.H. and G.H. are supported by the startup funding of University of Massachusetts. Open access funding enabled and organized by Projekt DEAL.

Conflict of interest

The authors declare no conflict of interest.

Keywords: bodipy · intersystem crossing · photodynamic therapy · photosensitizers · twisted π-systems

[1] D. E. Dolmans, D. Fukumura, R. K. Jain, *Nat. Rev. Cancer* **2003**, *3*, 380 – 387.
[2] J. F. Lovell, T. W. Liu, J. Chen, G. Zheng, *Chem. Rev.* **2010**, *110*, 2839 – 2857.
[3] M. R. Detty, S. L. Gibson, S. J. Wagner, *J. Med. Chem.* **2004**, *47*, 3897 – 3915.
[4] R. Lincoln, L. Kohler, S. Monro, H. Yin, M. Stephenson, R. Zong, A. Chouai, C. Dorsey, R. Hennigar, R. P. Thummel, *J. Am. Chem. Soc.* **2013**, *135*, 17161 – 17175.
[5] J. Li, K. Pu, *Acc. Chem. Res.* **2020**, *53*, 752 – 762.
[6] D. Van Straten, V. Mashayekhi, H. S. De Bruijn, S. Oliveira, D. J. Robinson, *Cancers* **2017**, *9*, 19.
[7] T. J. Dougherty, C. J. Gomer, B. W. Henderson, G. Jori, D. Kessel, M. Korbelik, J. Moan, Q. Peng, *J. Natl. Cancer Inst.* **1998**, *90*, 889 – 905.
[8] D. Sarezky, A. R. Raquib, J. L. Dunaief, B. J. Kim, *Clin. Ophthalmol.* **2016**, *10*, 1899 – 1903.
[9] N. J. Turro, V. Ramamurthy, J. C. Scaiano, *Principles of Molecular Photochemistry: An Introduction*, University Science Books, Sausalito, CA, **2009**.
[10] J. Zhao, W. Wu, J. Sun, S. Guo, *Chem. Soc. Rev.* **2013**, *42*, 5323 – 5351.
[11] S. Campagna, F. Puntoriero, F. Nastasi, G. Bergamini, V. Balzani, *Top. Curr. Chem.* **2007**, *280*, 117 – 214.
[12] Y. You, W. Nam, *Chem. Soc. Rev.* **2012**, *41*, 7061 – 7084.
[13] I. Eryazici, C. N. Moorefield, G. R. Newkome, *Chem. Rev.* **2008**, *108*, 1834 – 1895.
[14] S. Ji, W. Wu, W. Wu, H. Guo, J. Zhao, *Angew. Chem. Int. Ed.* **2011**, *50*, 1626 – 1629; *Angew. Chem.* **2011**, *123*, 1664 – 1667.
[15] Y. Chi, P.-T. Chou, *Chem. Soc. Rev.* **2007**, *36*, 1421 – 1431.
[16] A. Gorman, J. Killoran, C. O'Shea, T. Kenna, W. M. Gallagher, D. F. O'Shea, *J. Am. Chem. Soc.* **2004**, *126*, 10619 – 10631.
[17] Y. Hou, Q. Liu, J. Zhao, *Chem. Commun.* **2020**, *56*, 1721 – 1724.
[18] K. Nagarajan, A. R. Mallia, K. Muraleedharan, M. Hariharan, *Chem. Sci.* **2017**, *8*, 1776 – 1782.
[19] C. A. Salla, G. Farias, M. Rouzières, P. Dechambenoit, F. Durola, H. Bock, B. de Souza, I. H. Bechtold, *Angew. Chem. Int. Ed.* **2019**, *58*, 6982 – 6986; *Angew. Chem.* **2019**, *131*, 7056 – 7060.
[20] K. Liu, R. A. Lalancette, F. Jäkle, *J. Am. Chem. Soc.* **2017**, *139*, 18170 – 18173.
[21] J. W. Arbogast, A. P. Darmanyan, C. S. Foote, F. Diederich, R. Whetten, Y. Rubin, M. M. Alvarez, S. J. Anz, *J. Phys. Chem.* **1991**, *95*, 11 – 12.
[22] W. Hu, T. He, H. Zhao, H. Tao, R. Chen, L. Jin, J. Li, Q. Fan, W. Huang, A. Baev, *Angew. Chem. Int. Ed.* **2019**, *58*, 11105 – 11111; *Angew. Chem.* **2019**, *131*, 11222 – 11228.
[23] Z. Yu, Y. Wu, Q. Peng, C. Sun, J. Chen, J. Yao, H. Fu, *Chem. Eur. J.* **2016**, *22*, 4717 – 4722.
[24] Y. Wu, Y. Zhen, Y. Ma, R. Zheng, Z. Wang, H. Fu, *J. Phys. Chem. Lett.* **2010**, *1*, 2499 – 2502.
[25] S. Menning, M. Krämer, A. Duckworth, F. Rominger, A. Beeby, A. Dreuw, U. H. F. Bunz, *J. Org. Chem.* **2014**, *79*, 6571 – 6578.
[26] K. Nagarajan, A. R. Mallia, V. S. Reddy, M. Hariharan, *J. Phys. Chem. C* **2016**, *120*, 8443 – 8450.
[27] K. Schmidt, S. Brovelli, V. Coropceanu, D. Beljonne, J. Cornil, C. Bazzini, T. Caronna, R. Tubino, F. Meinardi, Z. Shuai, *J. Phys. Chem. A* **2007**, *111*, 10490 – 10499.
[28] S. Kim, S. Weissman, *J. Am. Chem. Soc.* **1979**, *101*, 5863 – 5864.
[29] T. Biet, K. Martin, J. Hankache, N. Hellou, A. Hauser, T. Bürgi, N. Vanthuyne, T. Aharon, M. Caricato, J. Crassous, *Chem. Eur. J.* **2017**, *23*, 437 – 446.
[30] Y.-C. Hsieh, C.-F. Wu, Y.-T. Chen, C.-T. Fang, C.-S. Wang, C.-H. Li, L.-Y. Chen, M.-J. Cheng, C.-C. Chueh, P.-T. Chou, *J. Am. Chem. Soc.* **2018**, *140*, 14357 – 14366.
[31] I. H. Delgado, S. Pascal, A. Wallabregue, R. Duwald, C. Besnard, L. Guénée, C. Nançoz, E. Vauthey, R. C. Tovar, J. L. Lunkley, *Chem. Sci.* **2016**, *7*, 4685 – 4693.
[32] H. Ito, H. Sakai, Y. Suzuki, J. Kawamata, T. Hasobe, *Chem. Eur. J.* **2020**, *26*, 316 – 325.
[33] Y. Hayashi, N. Obata, M. Tamaru, S. Yamaguchi, Y. Matsuo, A. Saeki, S. Seki, Y. Kureishi, S. Saito, S. Yamaguchi, *Org. Lett.* **2012**, *14*, 866 – 869.
[34] J. Wang, Q. Wu, S. Wang, C. Yu, J. Li, E. Hao, Y. Wei, X. Mu, L. Jiao, *Org. Lett.* **2015**, *17*, 5360 – 5363.
[35] Z. Zhou, J. Zhou, L. Gai, A. Yuan, Z. Shen, *Chem. Commun.* **2017**, *53*, 6621 – 6624.
[36] M. Gingras, *Chem. Soc. Rev.* **2013**, *42*, 1051 – 1095.
[37] J. K. Zak, M. Miyasaka, S. Rajca, M. Lapkowski, A. Rajca, *J. Am. Chem. Soc.* **2010**, *132*, 3246 – 3247.
[38] T. J. Wigglesworth, D. Sud, T. B. Norsten, V. S. Lekhi, N. R. Branda, *J. Am. Chem. Soc.* **2005**, *127*, 7272 – 7273.
[39] A. Loudet, K. Burgess, *Chem. Rev.* **2007**, *107*, 4891 – 4932.
[40] J. Zhao, K. Xu, W. Yang, Z. Wang, F. Zhong, *Chem. Soc. Rev.* **2015**, *44*, 8904 – 8939.
[41] S. Ji, W. Wu, W. Wu, P. Song, K. Han, Z. Wang, S. Liu, H. Guo, J. Zhao, *J. Mater. Chem.* **2010**, *20*, 1953 – 1963.
[42] S. Guo, K.-K. Chen, R. Dong, Z.-M. Zhang, J. Zhao, T.-B. Lu, *ACS Catal.* **2018**, *8*, 8659 – 8670.
[43] A. A. Granovsky, Firefly version 8.0.0, http://classic.chem.msu.su/gran/firefly/index.html **2014**.
[44] M. W. Schmidt, K. K. Baldridge, J. A. Boatz, S. T. Elbert, M. S. Gordon, J. H. Jensen, S. Koseki, N. Matsunaga, K. A. Nguyen, S. Su, T. L. Windus, M. Dupuis, J. A. Montgomery, Jr., *J. Comput. Chem.* **1993**, *14*, 1347 – 1363.
[45] M. Mitsunaga, M. Ogawa, N. Kosaka, L. T. Rosenblum, P. L. Choyke, H. Kobayashi, *Nat. Med.* **2011**, *17*, 1685 – 1691.
[46] A. Swaika, W. A. Hammond, R. W. Joseph, *Mol. Immunol.* **2015**, *67*, 4 – 17.
[47] L. Hu, Z. Cao, L. Ma, Z. Liu, G. Liao, J. Wang, S. Shen, D. Li, X. Yang, *Biomaterials* **2019**, *223*, 119469.

[48] A. P. Castano, M. Pawel, M. R. Hamblin, *Nat. Rev. Cancer* **2006**, *6*, 535 – 545.
[49] S. O. Gollnick, S. S. Evans, H. Baumann, B. Owczarczak, P. Maier, L. Vaughan, W. C. Wang, E. Unger, B. W. Henderson, *Br. J. Cancer* **2003**, *88*, 1772 – 1779.
[50] L. Galluzzi, O. Kepp, G. Kroemer, *EMBO J.* **2012**, *31*, 1055 – 1057.
[51] L. Milla Sanabria, M. E. Rodríguez, I. S. Cogno, N. B. R. Vittar, M. F. Pansa, M. J. Lamberti, V. A. Rivarola, *Biochim. Biophys. Acta Rev. Cancer* **2013**, *1835*, 36 – 45.
[52] L. Ni, J. Lu, *Cancer Med.* **2018**, *7*, 4509 – 4516.
[53] G. Lan, K. Ni, Z. Xu, S. S. Veroneau, Y. Song, W. Lin, *J. Am. Chem. Soc.* **2018**, *140*, 5670 – 5673.

Manuscript received: April 11, 2020
Version of record online: June 30, 2020

